Journal of Manufacturing Engineering, December 2010, Vol. 5, Issue 4, pp 309-315

MICROSTRUCTURE AND MECHANICAL PROPERTIES OF LASER BEAM WELDED AISI 409M GRADE FERRITIC STAINLESS STEEL JOINTS

***Lakshminarayanan A K[1] and Balasubramanian V[2]**

[1, 2] Department of Manufacturing Engineering, Annamalai University, Annamalai Nagar, Tamilnadu- 608002, India

ABSTRACT

This paper deals with the microstructure analysis and mechanical properties evaluation of laser beam welded AISI 409M ferritic stainless steel joints. Single pass autogeneous welds free of volumetric defects were produced at a welding speed of 3000 mm/min. The joints were subjected to optical microscopy, scanning electron fractography, microhardness, transverse and longitudinal tensile, bend and charpy impact toughness testing. The coarse ferrite grains in the base metal were changed into dendritic grains as a result of rapid solidification of laser beam welds. Tensile testing indicates overmatching of the weld metal relative to the base metal. The joints are also exhibited acceptable impact toughness and bend strength properties.

Keywords: *Laser Beam Welding, Ferritic Stainless Steel, Tensile Property and Impact Property.*

1. Introduction

The 409M grade is widely applied to construct coal wagons used for transporting iron ore [1]. The steel was developed from the ferritic stainless steel AISI 409 by careful balancing of ferrite (Cr, Si, Ti) and austenite (Ni, Mn, C, N) stabilising elements using Kaltenhauser's relationship presented in Eq.1 [2].

$$\text{Kaltenhaus er Ferrite Factor (KFF)} = Cr + 6Si + 8Ti - 2Mn - 4Ni - 40(C + N) \quad (1)$$

Though this modified 12 % Cr ferritic stainless steels are having better weldability than conventionally used ferritic stainless steels, the steel still suffers from grain growth in the heat affected zone (HAZ) and fusion zone (FZ), which results in significant alterations in the mechanical properties [3,4].

Due to the high energy density, laser beam welding is attractive for ferritic stainless steel, because of the narrow width of the fusion zone and heat affected zone [5]. The general attributes of a laser beam weld are that the relative heat input is low compared to other welding processes, and therefore the cooling rate is relatively high [6]. The inherent rapid solidification makes the use of lasers very attractive because completed welds contain a range of microstructures with metastable and stable phases, minimum segregation and fine grain sizes which often improve the mechanical properties [7]. Conventional arc welding characteristics of ferritic stainless steels have been examined by several researchers [8–11]. However, data on high energy density processes such as laser beam (LB) welding of ferritic stainless steel are scarce. The properties of laser and electron beam welded high chromium ferritic stainless steel was investigated by T.Mullin [12] and reported that the laser beam welded ferritic steel joints exhibited excellent impact toughness and corrosion resistance. Rakesh Kaul et al.,[13] studied the low heat input characteristics of laser welding to effectively control grain coarsening in the FZ and HAZ of 1.2-mm thick stabilized 17 wt % Cr ferritic stainless steel weldment. Taban et al,[14] investigated the properties of laser welded modified X2CrNi12 ferritic stainless steel and it was found that the grain coarsening has no adverse effect on tensile and bend nor on fatigue properties and has negative effect on impact toughness. However reported literature on laser beam welding of ferritic stainless is very scant and no systematic study has been reported on correlating microstructure and mechanical properties of laser beam welded 409M ferritic stainless steel joints. By pondering this in mind, the present study is focused on evaluating the microstructure, microhardness, tensile, impact, and bend strength of laser beam welded 409M ferritic stainless steel.

2. Experimentation

The as-received base material (BM) used in this study was 4 mm thick cold rolled, annealed and pickled AISI 409M grade ferritic stainless steel plates. The chemical composition of the base metal presented Table 1 was obtained using a vacuum spectrometer (ARL,

**Corresponding Author - E- mail: akln2k2@yahoo.com*

model 3460). Sparks were ignited at various locations, and their spectrum was analyzed for the estimation of alloying elements. Few welding trials were carried out in square butt configuration using 3.5 kW CO2 laser welding system (Make: Rofin, Germany; Model: #DC-035) and specimens were extracted from various locations of the joint and subjected to macrostructural analysis.

Table 1: Chemical Composition of Base Metal

C	Cr	Ni	Nb	Cu	Si	Mn
0.028	11.00	0.4	0.009	0.365	0.45	1.15

P	S	N	Al	Co	Ti
0.4	0.16	0.04	0.01	0.2	0.008

The specimen free of volumetric defect and full penetration was considered as the optimized welding condition. To limit the formation of plasma above the weld pool, pure helium was used as the shielding gas during welding to prevent oxidation of plate surface. Argon, which has a lower ionization potential than helium, is more prone to plasma formation above the weld pool. Plasma formation is highly undesirable, since it tends to deflect the laser beam reducing the depth of penetration [15]. The welding conditions and optimized process parameters presented in Table 2 were used to fabricate the joints for further investigation.

Table 2: Welding Conditions

Parameters	Values
Focal length (mm)	300
Power (kW)	3.5
Welding speed (mm/min)	3000
Shielding gas (litres/min)	30
Focal spot diameter (μm)	180

The photograph of laser welded 409M ferritic stainless steel joint is displayed in Fig. 1. The welded joints were sliced (as shown in Fig. 2) using abrasive cutting and then machined to the required dimensions for preparing tensile, charpy impact, bend and metallographic specimens.

Two different tensile specimens were prepared to evaluate the transverse tensile properties. Un-notched smooth tensile specimens were prepared to evaluate the transverse tensile properties of the joints such as yield strength, tensile strength and elongation. Notched specimens were prepared to evaluate notch tensile strength and notch strength ratio (notched tensile strength/un-notched tensile strength) of the joints. Flat micro tensile specimens prepared from the weld metal region were used to evaluate the all weld metal tensile properties. Three replicates for tensile testing were prepared to minimize errors. Tensile testing was carried out using 100 kN, electromechanical controlled universal testing machine (Fie-Blue Star, India; model Unitek-94100). ASTM E8M-04 guidelines were followed for preparing and testing the tensile specimens.

Fig. 1 Joint Photograph

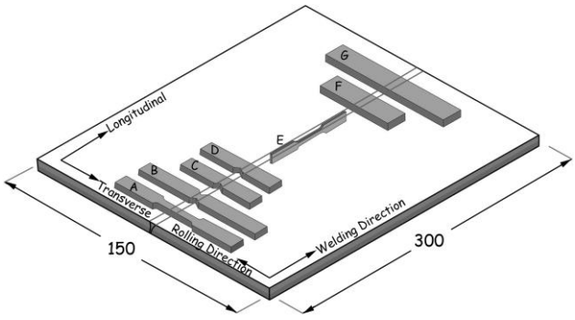

Fig. 2 Scheme of Extraction of Specimens for Mechanical Testing

(A-Smooth tensile specimen, B- Notched tensile specimen, C & D– Impact specimen notch placed at the weld centre and HAZ respectively, E- Longitudinal tensile specimen, F- Metallographic specimen, G - bend test specimen)

Charpy impact specimens were prepared to evaluate the impact toughness of the weld metal and HAZ, and hence the notch was placed (machined) at the weld metal (weld centre) as well as in the HAZ. As the plate thickness is small, subsized specimens were prepared. Impact testing was conducted at room temperature using a pendulum-type impact testing

machine (Enkay, India) with a maximum capacity of 300 J. The amount of energy absorbed in fracture was recorded, and the absorbed energy is defined as the impact toughness of the material. ASTM E23-04 specifications were followed for preparing and testing the impact specimens. Face and root three-point bend tests were performed as per ASTM E190-03 specifications. A Vickers microhardness testing machine (Shimadzu, Japan; model HMV-2T) was used for measuring the hardness of the weld with 0.05 kg load and with a dwell time of 15 sec. Microstructural examination was carried out using an optical microscope (Meji, Japan; model MIL-7100) incorporating image analysing software (Metal vision). The specimens for metallographic examination were sectioned to the required size from the joint comprising weld metal, HAZ and base metal regions, and polished using different grades of emery papers. Final polishing was done using a diamond compound (1 mm particle size) in the disc polishing machine. The specimens were etched with standard vilelia's reagent for 30 s. The fractured surface of the tensile and impact tested specimens was analyzed using a scanning electron microscope (Jeol, Japan; model 6410LV) at higher magnification to study the fracture morphology and establish the nature of the fracture.

3. Results

3.1 Macrostructure

Macrostructure of the laser beam welded 409M grade FSS joint is shown in Fig. 3. The weld cross-section has no volumetric defect. The macrostructure of the joint can be split into four distinct regions such as fusion zone (FZ), high temperature heat affected zone (HTHAZ), low temperature heat affected zone (LTHAZ) and the base metal (BM)

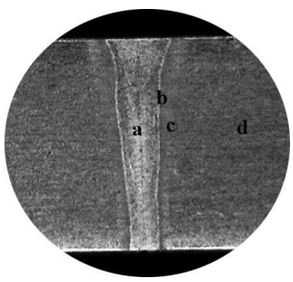

Fig. 3 Macrostructure of Laser Beam Welded 409M Ferritic Stainless Steel

(a – Fusion zone, b- higher temperature heat affected zone, c – Low temperature heat affected zone d – Base metal).

3.2 Microstructure

Optical micrographs of base metal and at different regions of LBW joint are displayed in Fig. 7. The base metal (Fig. 7a) exhibits a microstructure of coarse ferrite grains approximately 30 μm in diameter with randomly distributed carbides. The laser beam weld metal consisted largely of dendritic grains formed by rapid solidification (Fig. 7c). LB welds contain dendritic grains at the outer portion with equiaxed axial grains in the central regions (Figs. 7b & 7e).

3.3 Tensile and bend properties

Transverse tensile properties such as yield strength, tensile strength and fracture elongation of the three joints were evaluated and average results are presented in Table 3. Laser beam welded 409M joint was overmatched relative to the base metal. The ultimate tensile strength of base metal and laser beam welded joint are 536 MPa and 548 MPa respectively. Notch tensile strength of the welded joint is 764 MPa. Since the tensile specimens involving the entire joint shown in Fig. 4 fractured in the base metal region, flat micro tensile longitudinal tensile specimen were used to characterize the tensile properties of the weld metal region. In this case, the 0.2% proof strength and ultimate tensile strength are 412 MPa and 704 MPa respectively. The fracture elongation of all weld metal of laser beam welded 409M joint is 16 % lesser compared with the base metal. Fig. 5 shows the root and face bent specimen of the as-welded joints. Bend test results indicated the excellent ductility of LBW joint. There are no visible cracks in the cross section of weld region.

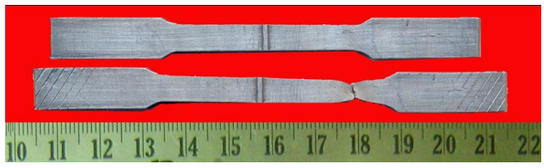

Fig. 4 Fracture of Tensile Specimens

3.4 Hardness

The micro hardness across the mid thickness of the welded joint was measured and presented in Fig. 6. The hardness of the as-received base metal is approximately 170 HV. The hardness of the fusion zone varies from 290 to 325 HV, depending on the grain size and phases sampled by each indentation.

3.5 Impact toughness

Charpy impact toughness of the LBW joint was evaluated and presented in Table 3. The impact

toughness of unwelded base metal is 34 J, However, the impact toughness of LBW joint with notch placed at the weld centerline and HAZ region are 35 J and 29 J respectively.

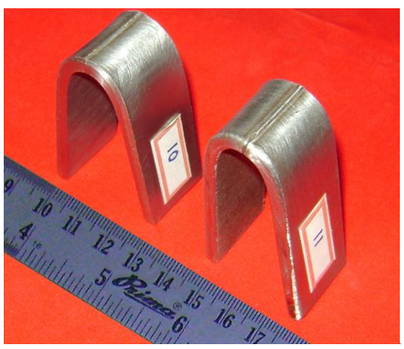

Fig. 5 Root and Face Bent Specimens

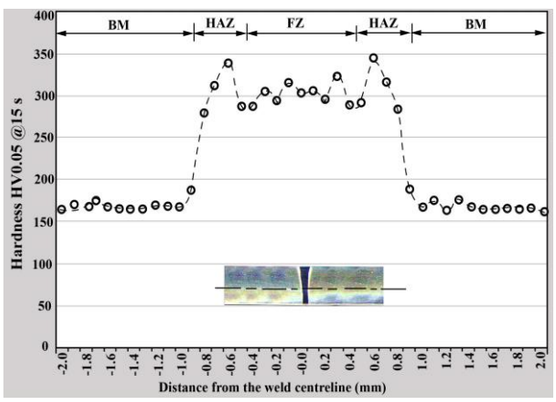

Fig. 6 Hardness Profile at Mid Cross Section

3.6 Fractography

Fig. 8 displays the fractographs of tensile and impact tested specimens of base metal and laser welded 409M FSS joints. The displayed fractographs invariably consist of dimples, which are an indication that most of the tensile test specimens failed in a ductile manner under the action of tensile loading. However, finer dimples were observed in LBW joints compared with the base metal.

4. Discussion

Transverse tensile properties of the base metal and welded joint are presented in Table 3. The weld metal region has the higher ultimate tensile strength (UTS) and 0.2% offset yield strength (YS), and lower elongation than the BM. The transverse tensile specimen of the joint fractured in the BM region, because the BM had the lowest hardness, as shown in Fig. 6. The strength is roughly proportional to hardness, so that the BM region would preferentially yield and then fail during transverse tensile test. Flat microtensile specimens were used to determine the all weld metal tensile properties. Substantial differences in strength properties (mismatching) of the base metal and narrow fusion zone of the LB welds inevitably occur due to the rapid thermal cycle of the joining process. The overall mechanical properties of a weld are determined by the characteristic properties of the individual microstructures present in the weld zone and the heat-affected zone of LBW joint. The fusion zone of the laser beam weld consists of dendritic columnar grains and axial grains (Fig. 7b & 7e). The thermal conductivity of ferritic stainless steel is being higher; the heat flow in the direction perpendicular to the weld would be maximum. Therefore, the grains tend to grow in that direction, giving rise to columnar grains. The columnar dendritic structure of the grains observed on the ferritic stainless steel is in conformity with general trends reported for such welds [16, 17]. Axial grains initiate in the original weld bead and grow along the length of the weld, blocking the columnar grains growing in from the fusion lines. Axial grains observed in laser beam welds are due to the fact that this is the last region to solidify, and this type of grain structure is consistent with trends reported in welds [18].

When considering a weld cross section, each point at a given distance from the weld centre line experiences a different peak temperature and cooling rate. As the distance from the weld centre line increases, the peak temperature and cooling rate decrease and this influences the microstructure that develops [19]. The fusion zone and high temperature heat affected zone (heated above about 1300^{o}C) reaches the δ ferrite range and considerable grain growth takes place at high temperatures in case of conventional arc welding. However, a characteristic feature of the laser beam 409M ferritic stainless steel welds was the virtual absence of grain growth in the HAZ. The problem of extensive grain coarsening and associated brittleness often cited in the welding of ferritic stainless steels by arc processes is essentially absent from laser beam welding process. The grain size in the HTHAZ of the LB welds was found to be very similar to that of the BM with low carbon grain boundary martensite. This phenomenon is due to the relatively low heat input associated with laser beam welding. During cooling through the austenite formation ranges, a considerable amount of austenite formed at the grain boundaries, which are determined by the relative amount of ferrite and austenitic stabilizing elements and the cooling rate.

Table 3: Tensile and Impact Property of LBW Joints in Comparison with the Base Metal.

Joint	Yield Strength (MPa)	Tensile Strength (MPa)	Elongation (%)	Notch Tensile Strength (MPa)	Notch Strength Ratio (NSR)	Impact Toughness (J)		Joint efficieny (%)
						WM	HAZ	
BM	352 (5.2)	536 (4.1)	31 (0.94)	662 (7.2)	1.24	34 (0.8.)		---
LBW Joint	382 (4.3)	546 (2.9)	32 (1.3)	764 (4.6)	1.34	35(1.8)	27 (2.5)	102
LBW- All Weld	412 (2.1)	704 (3.1)	29 (0.8)	---	---	---	---	---

Note: Values given in the brackets are standard deviation of experimental results

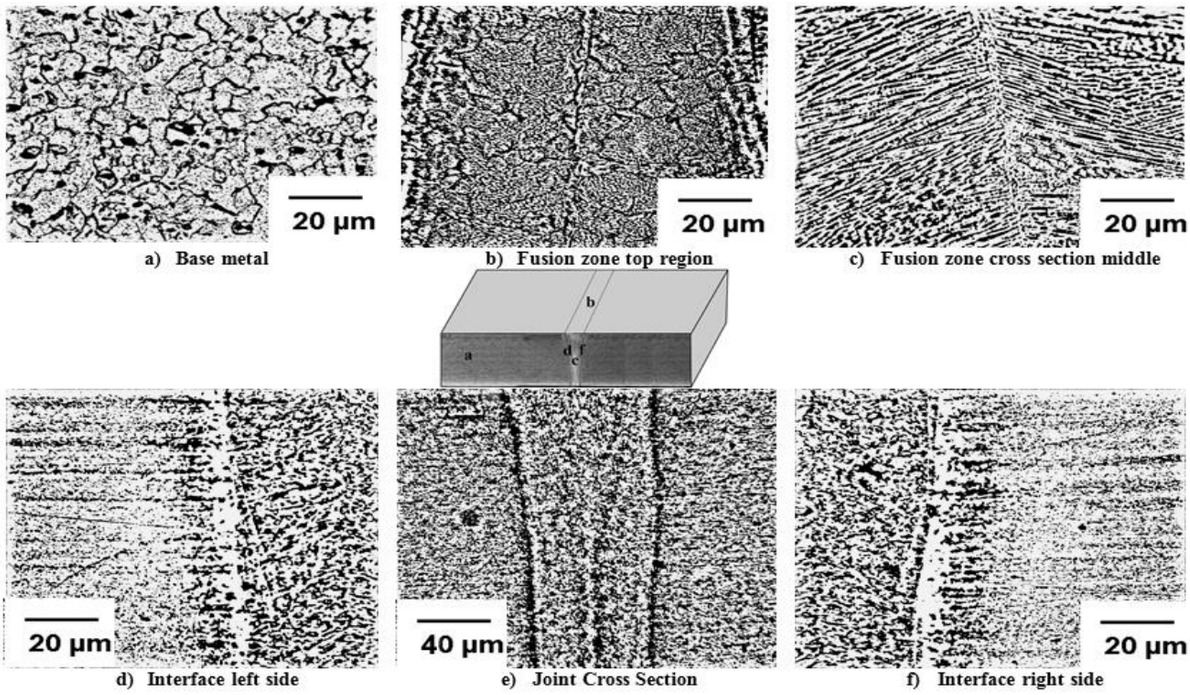

Fig. 7 Optical Micrographs of Laser Beam Welded 409M Ferritic Stainless Steel Joint

If the cooling rate is not excessive, the austenite has time to grow and cover all available ferrite grain boundaries. However, under the rapid cooling rates associated with LBW, transformation to austenite was fairly suppressed leading to a predominantly ferritic structure accompanied with continuous networks of martensite along the grain boundaries. The steel used in this study is not sufficiently alloyed for the austenite to remain stable down to room temperature, therefore it transforms to low carbon lath martensite. It has been found that when levels of ferrite are increased, there is less austenite available at high temperature for the solution of carbon which can lead to chromium carbide precipitation. A much wider duplex zone with tough fine grained ferrite and low carbon lath martensite right next to coarse grained zone, (Fig. 7d & 7f) was observed. This wider low temperature heat affected duplex zone originated when the material was heated to temperatures (900ºC – 1300ºC) within the dual phase ferrite and austenite phase field. The maximum amount of martensite formed at the point in this zone at which the longest time was spent during welding and at the temperature of 1050ºC at which the maximum amount of austenite will form.

The presence of hard untempered martensite would reduce the ductility of the weld and could act as stress raisers and crack initiation points [20]. However, one of problems plaguing ferritic stainless steels is rapid grain growth at high temperature with subsequent brittleness, and substantial transformation of austenite and martensite during cooling will result in significant grain refinement and improvement in toughness [21]. Since weld microstructure is greatly influenced by chemical composition, the chromium equivalent and nickel equivalent based on Balmforth and Lippold constitutional diagram [22] for ferritic-martensitic stainless steel are calculated by using the equations *2* and *3*.

$$Cr_{Eq} = Cr + 2Mo + 10(Al + Ti) \quad (2)$$

$$Ni_{Eq} = Ni + 35C + 20N \quad (3)$$

By plotting Cr-Eq and Ni-Eq values on the constitution diagram, approximately 80 % ferrite and 20 % martensite is expected in the weld metal. Grain refinement of ferritic stainless steel weldments will substantially increase the tensile and impact properties [23]. The grain sizes of the LB-weld metal and HAZ were finer than those of the BM as a result of characteristic rapid solidification. The better strength and toughness of 409M laser beam welds could be due to a fine solidification structure as a result of fast solidification and is due to a combination of equiaxed and columnar grain perpendicular to the crack path.

5. Conclusions

The microstructure and mechanical properties of laser beam welded AISI 409M ferritic stainless steel joints were investigated. From this investigation the following important findings are derived:

i. The coarse ferrite grains in the base material are changed to fine columnar dendritic grains and equiaxed axial grains of ferrite with some grain boundary lath martensite as a result of rapid solidification of laser beam welds.

ii. Tensile strength of laser beam weld metal is found to be 31 % higher compared to the tensile strength of base material.

iii. The hardness of the fusion zone was varying from 290 to 325 HV, which was higher than the base material (170 HV). This is mainly due to fine solidification structure as a result of fast solidification.

iv. The impact toughness of 409M laser beam welds is 3% greater compared to the base metal and it is due to the presence of equiaxed and columnar dendritic grain perpendicular to the crack path.

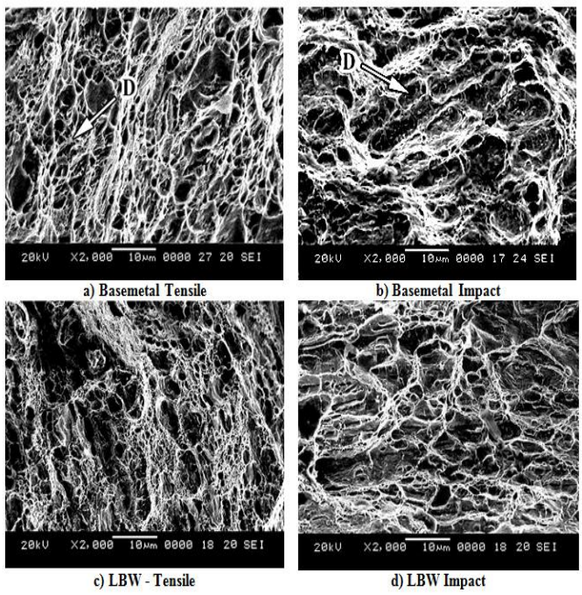

Fig. 8 SEM Fractographs of Tensile and Impact Tested Specimens

References

1. *AISI 409M – Technical Data (2004), "Detail Brochure Published by SAIL", India.*

2. *Kalthauser R H (1982), "Improving the Engineering Properties of Stainless Steels", Source Book on the Ferritic Stainless Steel. ASM Engineering Bookshelf, 212-218.*

3. *Van Warmelo M, Nolan D and Norrish J (2007), "Mitigation of Sensitisation Effects in Unstabilised 12% Cr Ferritic Stainless Steel Welds", Material Science Engineering A, Vol.464,157–169.*

4. *Du Toit M and Naude J (2009), "The Influence of Stabilization with Titanium on the Heat Affected Zone Sensitization of 11 to 12% Chromium Ferritic Stainless Steels Under Low Heat Input Welding Conditions", IIW Doc. IX-H-705-09,1-12.*

5. *Mpenasa and Crivela (2003), "Application of the Laser Welding Process to Low Thickness Stainless Steels". Welding International, Vol. 17,947–957.*

6. *Hwa Teng Lee, Jia Lin Wu (2009), "The Effects of Peak Temperature and Cooling Rate on the Susceptibility to Intergranular Corrosion of Alloy 690 by Laser Beam and Gas Tungsten Arc Welding", Corrosion Science, Vol.51, 439–445.*

7. *Kell J, Tyrer J R, Higginson R L and Thomson R C (2005), "Microstructural Characterization of Autogenous Laser Welds on 316L Stainless Steel using EBSD and EDS". Journal of Microscopy, Vol. 217, 67–173.*

8. *Li-xin Wanga, Chang-jiang Song, Feng-mei Sun, Li-juan Li and Qi-jie Zhai (2009), "Microstructure and Mechanical Properties of 12 wt.% Cr Ferritic Stainless Steel with Ti and Nb Dual Stabilization", Material Design, Vol.30, 49–56.*

9. *Meadows C and Fritz J D (2005), "Understanding Stainless Steel Heat Affected Zones", Welding Journal, Vol.84, 25–30.*

10. *Shanmugam K, Lakshminarayanan A K, and Balasubramanian V (2009), "Tensile and Impact Properties of Shielded Metal Arc Welded Ferritic Stainless Steel Joints". Journal of Material Science and Technology, Vol.45, 181-186.*

11. *Taban E, Deleu E, Dhooge A and Kaluc E (2007) "Gas Metal Arc Welding of Modified X2CrNi12 Ferritic Stainless Steel". Kovove. Mater. Metall. Mater. Vol.45, 67–73.*

12. *Tullmin M, Robinson FPA, Henning CAO, Strauss A and J L Grange (1989), "Properties of Laser-Welded and Electron- Beam Welded Ferritic Stainless Steel". J. S. AIr. Inst. Min. Metal, Vol. 89, 243-249.*

13. *Kaul R, Ganesh P, Nath A K, Triapthi P and Nandedkar R V (2003), "Comparison of Laser and Gas Tungsten Arc Weldments of Stabilized 17 wt% Cr Ferritic Stainless Steel", Materials and Manufacturing Processes,Vol.18, 563–580.*

14. *Taban E, Deleu E, Dhooge A and Kaluc E (2009), "Laser Welding of Modified 12% Cr Stainless Steel: Strength, Fatigue, Toughness, Microstructure and Corrosion Properties". Material Design, Vol. 30, 1193–1200.*

15. *Angrezev (2005), "Plasma Formation in Laser Welding", Welding International, Vol.19, 808–813.*

16. *Madhusudhan Reddy G, Mohandas T, Sambasiva Rao A, and Satyanarayana A A (2007), "Influence of Welding Processes on Microstructure and Mechanical Properties of Dissimilar c Austenitic-Ferritic Stainless Steel Welds", Materials and Manufacturing Processes, Vol. 20, 147 - 173.*

17. *Madhusudan Reddy G and Srinivasa Rao K (2009), "Microstructure and Mechanical Properties of Similar and Dissimilar Stainless Steel Electron Beam and Friction Welds", International Journal of Advanced Manufacturing Technology, Vol. 45, 875–888.*

18. *Kaul R, Ganesh P, Nath A K, Triapthi P, and Nandedkar R V (2002), "Characterization and Comparison of Laser and Gas Tungsten Arc Weldments of AISI 430 Stainless Steel". Materials and Manufacturing Processes", Vol. 14 (1), 41–48.*

19. *Lippold J C and Kotecki D J (2005), "Welding Metallurgy and Weldability of Stainless Steels", New Jersey: John Wiley & Sons; 44-48.*

20. *Demo J J (1977), "Structure and Constitution of Wrought Ferritic Stainless Steels in Handbook of Stainless Steels". In: D. Peckner, I.M.Benstein (Eds), McGraw-HillBook Company, 5.1–5.40.*

21. *Topic M, Allen C and Tait R (2007), 'The Effect of Cold Work and Heat Treatment on the Fatigue Behavior of 3Cr12 Corrosion-Resistant Steel Wire". International Journal of Fatigue, Vol.29, 49-56.*

22. *Balmforth M C and Lippold J C (2007), "A New Ferritic–Martensitic Stainless Steel Constitution Diagram". Welding Journal, Vol. 77, 1s–7s.*

23. *Madhusudhan Reddy G and Mohandas T (2001), "Explorative Studies on Grain Refinement of Ferritic Stainless Steel Welds". Journal of Material Science Letters, Vol. 20, 721 – 723.*

